Diabatic Digital-Filtering Initialization: Application to the HIRLAM Model

XIANG-YU HUANG*

Department of Meteorology, Stockholm University, Sweden

PETER LYNCH

Meteorological Service, Dublin, Ireland

(Manuscript received 13 December 1991, in final form 9 April 1992)

ABSTRACT

A digital-filtering initialization scheme, which includes the effects of diabatic processes, has been formulated. This scheme gives a lower noise level in the forecast and a better organized initial pressure-tendency field than for the corresponding adiabatic initialization. The implementation of the scheme is very easy, requiring only the calculation of the filter coefficients and minor adjustments to the model code.

The computational expense of the digital-filtering initialization is directly proportional to the length of the time span over which the filter is applied. By a careful choice of filter weights, based on optimal filter theory, the span of the filter can be reduced by a factor of 2 or 3, with a corresponding increase in efficiency.

1. Introduction

Due to an imbalance between the mass and wind fields, large amplitude inertia–gravity oscillations occur in numerical models based upon primitive equations. Many initialization procedures have been developed to control these oscillations, for example, static initialization (Phillips 1960), dynamic initialization (Miyakoda and Moyer 1968), nonlinear normal-mode initialization (Machenhauer 1977; Baer 1977), and bounded derivative initialization (Semazzi and Navon 1986).

An alternative approach to the initialization methods mentioned above is to use time filters. A digital filter has been used to initialize data for a limited-area shallow-water model by Lynch (1990) and for a sophisticated baroclinic limited-area model by Lynch and Huang (1992, hereafter LH). In both studies, the numerical models are integrated forward and backward from the initial time. The time series of the model variables produced by the integrations are processed by a digital filter, which removes the high-frequency components from the initial data. The forward and backward integrations are performed adiabatically, that is, with all diabatic processes and horizontal diffusion disabled. The adiabatic digital-filtering initialization (ADFI) effectively removes the high frequencies while making very small changes to the initial fields and forecasts. In Lynch (1990), ADFI was compared to an initialization scheme based on the Laplace transform (Lynch 1985). The two schemes gave very similar results. In LH, ADFI was compared to the standard adiabatic nonlinear normal-mode initialization scheme (ANMI) of a high-resolution limited-area model (HIRLAM). The latter scheme uses the Machenhauer (1977) criterion, which sets the initial tendencies of the gravity modes to zero. Compared with the normal-mode scheme, ADFI gave superior results: there was less noise in the forecast and a more organized and synoptically reasonable initial pressure tendency field.

In this paper, the ADFI of LH is extended to include diabatic processes. The modified scheme will be referred to as diabatic digital-filtering initialization (DDFI). The basis of the method is outlined in section 2, and its application to specific cases is described in section 3. Optimal filters are introduced in section 4, and it is shown there how they may be used to improve the efficiency of DDFI. Some further results, using an optimal filter, follow in section 5. A discussion and conclusions are presented in section 6.

2. Basis of the DDFI method

The theoretical foundation of DDFI is the same as for ADFI in LH: the high frequencies are removed by applying a digital filter to a short time series generated by an integration from the initial data. The main dif-

* Present affiliation: Danish Meteorological Institute, Denmark.

Corresponding author address: Dr. Xiang-Yu Huang, Danish Meteorological Institute, Lyngbyvej 100, DK-2100 Copenhagen Ø, Denmark.

ference is that the time series of the model variables processed by the digital filter are produced by a diabatic integration of the model. In order for the time series to be centered around the initial time, an adiabatic integration is carried out backward in time for N time steps to produce a model state at $t = -N\Delta t$. Here the N-step numerical integration covers half of the total filter span $T_s = 2N\Delta t$, which extends from $-N\Delta t$ to $+N\Delta t$. From $t = -N\Delta t$, the model is integrated diabatically forward in time to $+N\Delta t$, giving a time series $X_d(n)$. The digital filter is then applied to $X_d(n)$, yielding a filtered field X_d^*:

$$X_d^* = \sum_{n=-N}^{N} h(-n)X_d(n), \tag{1}$$

where $h(n)$ are the filter coefficients. The filter used in section 3 is the same as that of LH, with coefficients given by

$$h(n) = \left\{\frac{\sin[n\pi/(N+1)]}{n\pi/(N+1)}\right\}\frac{\sin n\theta_c}{n\pi}. \tag{2}$$

Here θ_c is the cutoff digital frequency, which is related to the cutoff period τ_c:

$$\tau_c = \frac{\pi T_s}{N\theta_c}. \tag{3}$$

Further discussion and an alternative filter-design technique are presented in the Appendix.

When the model is diabatically integrated to the initial time, the model state $X_d(0)$ is generally different from the original analysis $X_a(0)$. An attempt to allow for this effect was made by defining a modified initialized field:

$$X^* = X_d^* - [X_d(0) - X_a(0)]. \tag{4}$$

It was found, however, that this modification diminished the effectiveness of the initialization, and it was therefore abandoned.

3. Results

a. Data and model

The first case chosen to demonstrate the DDFI method is the same one as was used in LH, in which an intense low crossed Denmark and southern Sweden on 5–6 September 1985. A discussion of the weather situation and numerical simulations of the storm can be found in Sundqvist et al. (1989). HIRLAM has a grid of 110 × 100 × 16 points, and a horizontal resolution 0.5° × 0.5° is used. The time step for the integration is 6 min. Both the filter span T_s and the cutoff period τ_c are chosen to be 6 h. The boundary values are fixed to their initial values during the initialization. A ten-point relaxation zone is used to ensure a smooth transition between the boundary and the interior values. A brief description of the model can be found in LH and more details are found in Källberg (1989).

b. Application of DDFI

The original analysis of the sea level pressure over the model domain for 0000 UTC 5 September 1985, is shown in Fig. 1a. The integration backward in time for 3 h yields a reasonable sea level pressure field (Fig. 1b). For instance, the troughs west of Ireland and in the Norwegian Sea have retrogressed, as might be expected. The trough in the Soviet Union (at 30°E) has intensified, while the low pressure centers over Sweden and England and the high pressure center south of Greenland have weakened slightly. During the backward integration, all the diabatic processes are switched off and horizontal diffusion is disabled. The boundary relaxation zone is also indicated in Fig. 1. The pressure field is smooth near the boundaries.

To produce the time series $X_d(n)$, a 6-h integration forward in time, with the fields $X_d(-N)$ as initial data, is performed with all the physical processes and the horizontal diffusion included. Applying the digital filter (1) to the time series $X_d(n)$, the resulting fields of DDFI are obtained. In Fig. 1c, the sea level pressure after DDFI is shown.

c. Reference experiments

There are three characteristics essential to any satisfactory initialization procedure: (i) high-frequency oscillations are removed from the forecast; (ii) changes made to the initial fields are acceptably small; and (iii) the forecast is not degraded by application of the initialization. A 24-h forecast from uninitialized data is carried out to serve as a reference so that the DDFI procedure can be evaluated in terms of these three requirements. The uninitialized initial analysis and subsequent forecast are denoted NOIN.

For the purpose of comparison, a parallel experiment using ADFI is performed. The model is adiabatically integrated backward 3 h and forward 3 h in time, giving a time series $X_a(n)$. Equation (1) is then applied to $X_a(n)$, yielding an ADFI initial analysis X_a^*. The only difference between the ADFI used here and that in LH is the boundary treatment. Instead of fixing the boundary values as in LH, the standard boundary relaxation scheme of HIRLAM is used (Källberg 1989).

d. Reduction of noise

The main objective of initialization is to remove the spurious high-frequency oscillations from a forecast. A common way to demonstrate the performance of an initialization scheme is to show the time evolution of the surface pressure and a midlevel vertical velocity at a model grid point (Williamson and Temperton 1981; Temperton and Williamson 1981). While the surface pressure is sensitive to noise in a vertically integrated sense, the midlevel vertical velocity indicates the internal noise. The time evolutions for the first 6 h of the forecast of the surface pressure p_s and 500-hPa

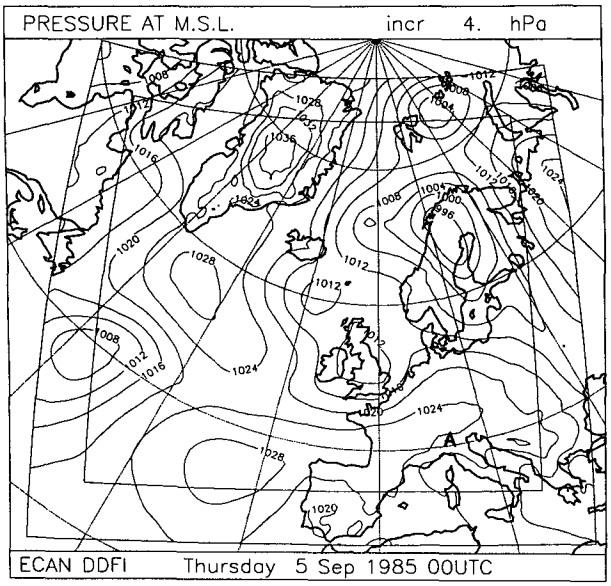

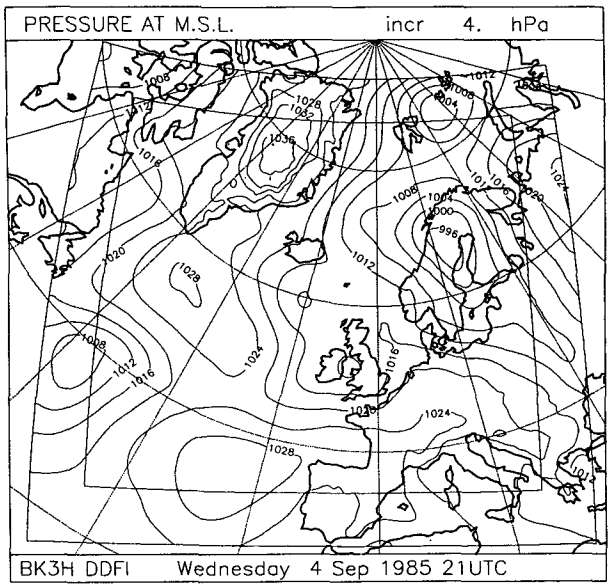

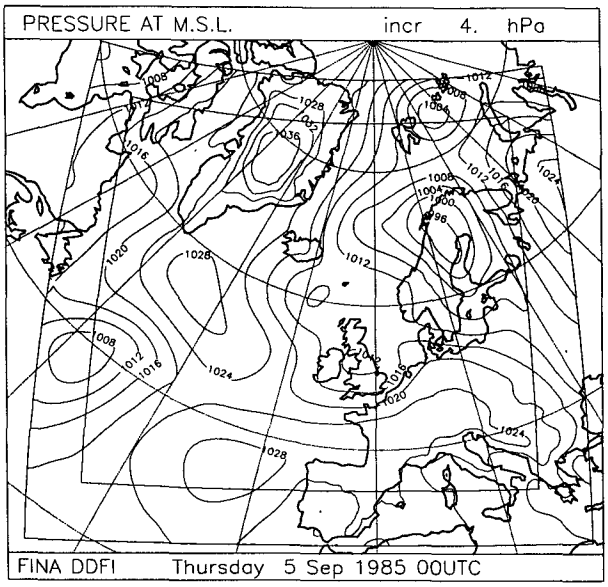

FIG. 1. (a) Uninitialized sea level pressure analysis (hPa) for 0000 UTC, 5 September 1985. (b) Sea level pressure after 3-h adiabatic integration backward in time. (c) Sea level pressure after DDFI. The limit of the boundary relaxation zone is shown in the figures.

vertical velocity $\omega = dp/dt$ at a model grid point in the Alps are shown in Fig. 2 and Fig. 3, respectively. The forecast starting from uninitialized analysis is severely contaminated by high-frequency oscillations, indicating a large imbalance in the initial mass and wind fields. Due to the damping mechanisms of the model (e.g., horizontal diffusion), a clear decrease is observed in the amplitude of the oscillations in p_s and ω in the first 6 h. The two forecasts from initialized analyses, however, have almost no high-frequency component in their evolution. The differences between DDFI and ADFI are small, less than 0.5 hPa in surface pressure p_s. The curves for the two initialized forecasts (DDFI and ADFI) in Fig. 2 are quite similar; it is difficult to tell which is better. There is a suggestion in Fig. 3 that the evolution of the 500-hPa vertical velocity is smoother for the diabatically initialized forecast; certainly, its initial variation is smaller.

In order to further compare DDFI and ADFI, the mean absolute surface pressure tendency N_1 is chosen to measure the global noise level. Here N_1 is defined as

$$N_1 = \frac{1}{IJ} \sum_{i=1}^{I} \sum_{j=1}^{J} \left| \frac{\partial p_s}{\partial t} \right|_{ij}, \tag{5}$$

where the summation is calculated over the inner model domain in the present study. In Fig. 4, the variation of N_1 during the first 6 h of the forecasts is shown. The three curves converge as the time integration is

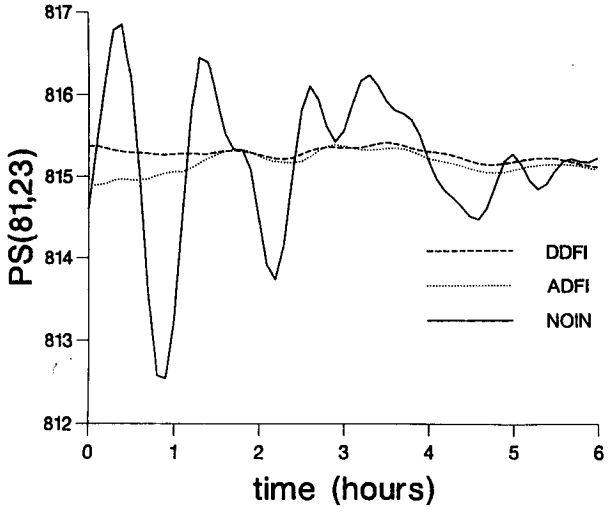

FIG. 2. Time evolution of surface pressure p_s (hPa) at a model grid point in the Alps (indicated by A in Fig. 1a).

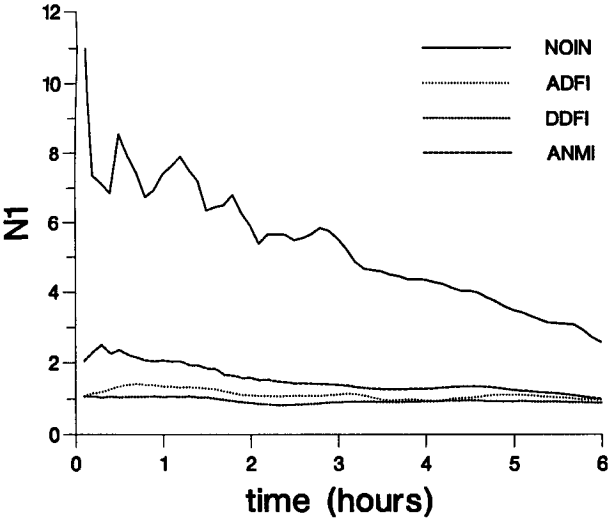

FIG. 4. Time evolution of the mean absolute surface pressure tendency averaged over the interior model domain [hPa (3 h)$^{-1}$].

carried on. In fact, there is almost no difference between them after 12 h. The distinct difference between the uninitialized forecast and the two initialized ones convincingly shows that the initial noise due to the imbalance between mass and wind fields is effectively removed by DDFI and ADFI procedures. Furthermore, the noise level for DDFI is slightly lower than for ADFI throughout the whole 6-h period of the integration. The fourth graph in Fig. 4 shows the variation of N_1 for the forecast starting from an analysis initialized using an adiabatic nonlinear normal-mode initialization (ANMI), described in LH. It can be seen that both DDFI and ADFI are superior to ANMI in reducing the high-frequency noise. A detailed comparison between ADFI and ANMI has been performed in LH and will not be repeated here.

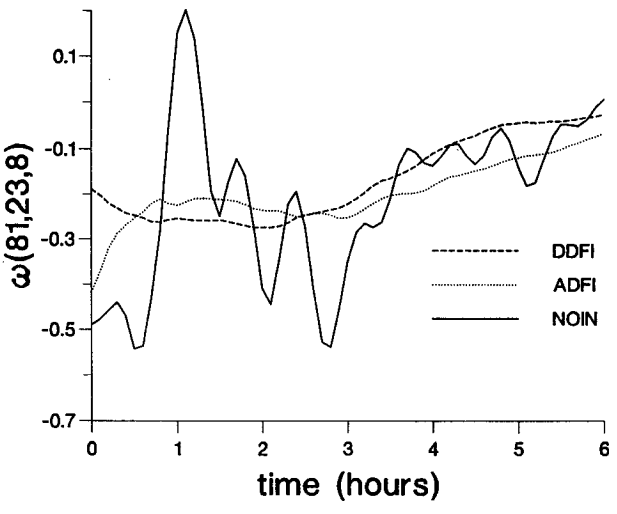

FIG. 3. Time evolution of 500-hPa vertical velocity ω (Pa s^{-1}) at a model grid point in the Alps (indicated by A in Fig. 1a).

In addition to areally averaged quantities, the initial surface pressure tendency maps are shown in Fig. 5. By means of DDFI (Fig. 5a) or ADFI (Fig. 5b), the noise is removed. The amplitude of the maximum pressure tendency is reduced to 3 hPa (3 h)$^{-1}$ in the interior domain and well-organized patterns on synoptic scales occur in accordance with the weather situation. For instance, minimum and maximum pressure tendency over the mid-Atlantic (Figs. 5a,b) are related to the development of the low and high pressure centers (cf., Fig. 1a). Compared to ADFI (Fig. 5b), the diabatic initialization scheme (Fig. 5a) gives an even smoother field, especially over the mountainous regions of Greenland, the Alps, and Scandinavia. A very noisy pressure-tendency field with a maximum of 130 hPa (3 h)$^{-1}$ was found in the uninitialized analysis (not shown here; see LH). This noise has been suppressed to some extent by ANMI (Fig. 5c); for example, the maximum is around 10 hPa (3 h)$^{-1}$ in Fig. 5c. However, this pressure-tendency field still contains small-scale features unrelated to the synoptic flow.

The surface pressure tendency is related to the vertically integrated divergence field. The improvements discussed above relate primarily to the reduction of noise in a vertically integrated sense. To evaluate the effect of the initialization on the internal modes, the divergence fields at each level are examined. The root-mean-square values of divergence, σ_δ, for the DDFI, ADFI, and NOIN analyses at each model level are shown in Fig. 6. Both the initialization schemes reduce σ_δ effectively. The reduction due to ADFI is of the order of 10%. The reduction brought about by DDFI is approximately twice as much. Since the divergence field is generally too large in the uninitialized analysis, this

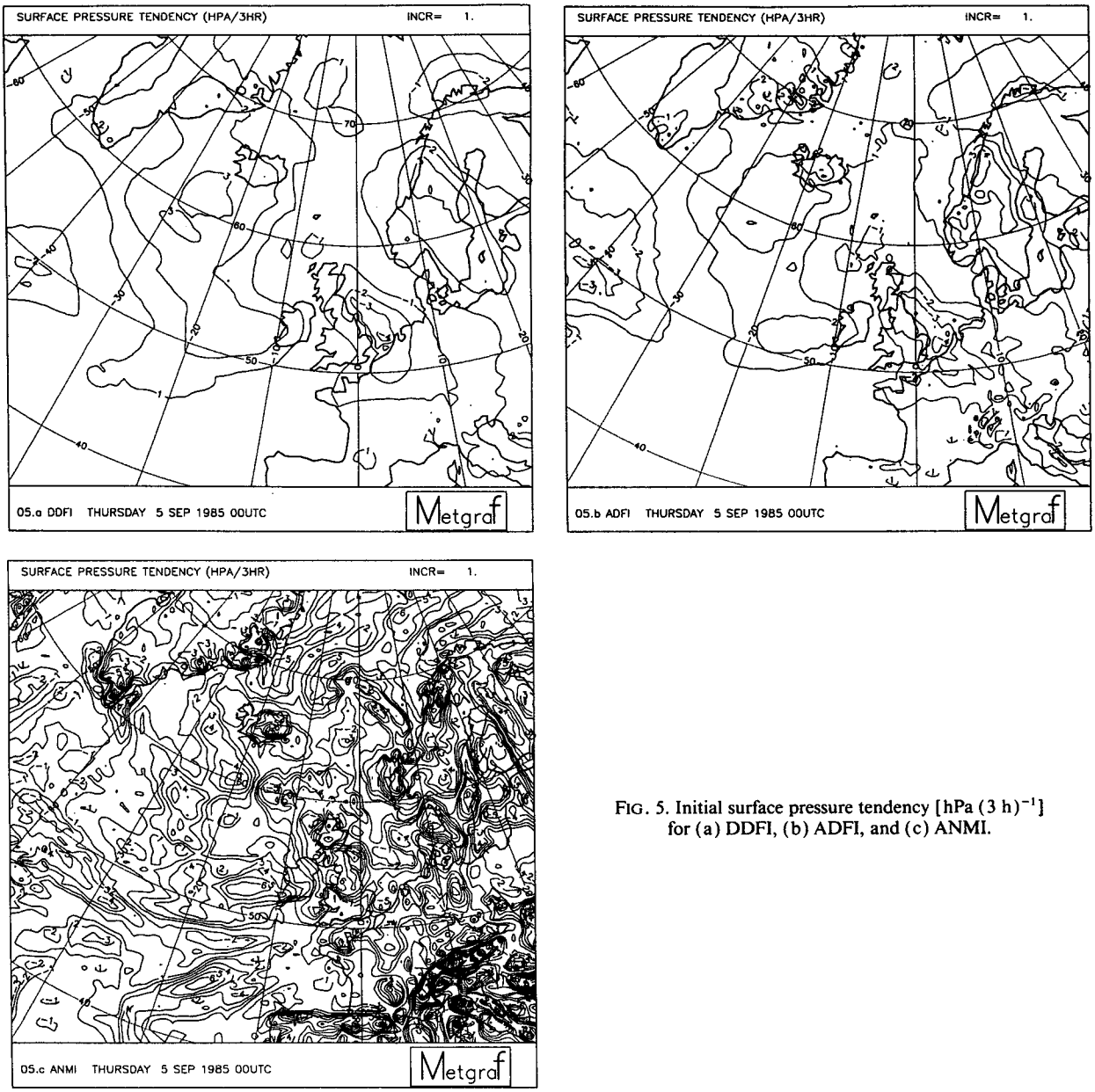

FIG. 5. Initial surface pressure tendency [hPa (3 h)$^{-1}$] for (a) DDFI, (b) ADFI, and (c) ANMI.

may be regarded as an improvement. The maximum difference between the reduction made by DDFI and that by ADFI occurs at the lowest model level, but this difference remains significant throughout the troposphere. (The changes in σ_δ due to ANMI were very small; see LH, Fig. 13.)

e. Changes made by DDFI to the model fields

The root-mean-square (rms) and maximum (max) differences in temperature, wind components, and surface pressure between the initialized and uninitialized analyses are shown in Table 1. The calculations of rms and max are confined to the interior region. The numbers in the table are reasonably small and generally less than the observational errors. Compared to the results of ADFI, the changes made by DDFI are somewhat larger but are still reasonably small (see Table 1). Similar calculations are made for the 24-h forecasts. The results in Table 2 show that DDFI does not affect the forecast very much if the uninitialized forecast is used as a reference. The changes made by ADFI and DDFI to the total potential energy (TPE) and the total kinetic energy (TKE) are also very small: +0.03% in TPE and −2% in TKE for DDFI; +0.01% in TPE and −1% in TKE for ADFI.

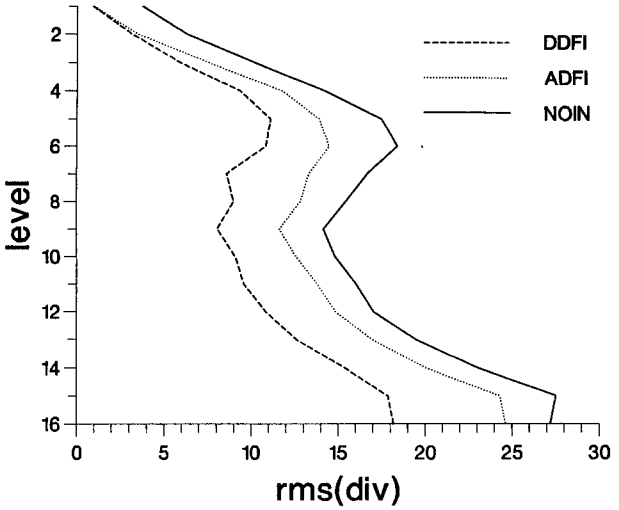

FIG. 6. Root-mean-square divergence (10^{-6} s^{-1}) as a function of model level for uninitialized analysis (full line), DDFI analysis (dashed line), and ADFI analysis (dotted line). The analysis was made at 0000 UTC 5 September 1985.

To give an idea of the spatial distribution of the changes made by DDFI, the differences in sea level pressure between DDFI and NOIN at the initial time and after 24 h are shown in Figs. 7a and 7b, respectively. The analysis changes are largest in the mountainous regions of Greenland and the Alps. At the end of the 24-h forecast, the difference between the DDFI forecast and the uninitialized forecast is very small; a 1-hPa contour line appears over Denmark. A close look at the 24-h sea level pressure forecast from DDFI analysis (Fig. 8a) and that from the uninitialized analysis (Fig. 8b) reveals that the change made by DDFI is actually a marginal improvement in the central pressure of the low, compared with the verifying analysis (Fig. 8c). The two forecasted low positions, however, are located at the same model grid points, which is about 100 km from that of the verifying analysis.

f. Spinup of precipitation

It is a common problem with numerical forecasts that the initial precipitation rate is either severely reduced or excessively high. The adjustment of precipitation and evaporation to a state of mutual balance is known as the model spinup. Attempts have been made to alleviate this problem by means of diabatic initialization. In a study by Kitade (1983), the diabatic nonlinear normal-mode initialization (DNMI) experiments made with the FSU (Florida State University) global spectral model suggest that DNMI provides a well-organized disturbance in the initial state followed by a larger amount of rainfall compared with ANMI. In another study by Wergen (1988), however, DNMI experiments made with the ECMWF (European Centre for Medium-Range Weather Forecasts) forecast system show little improvements in the spinup of the model precipitation. The diabatic dynamic initialization (DDI) technique recently formulated by Fox-Rabinovitz and Gross (1991) appears to be quite effective in reducing the initial spinup effect.

The initial precipitation rate and the 24-h accumulated precipitation pattern calculated from DDFI were not significantly different from those of ADFI. The two forecasts of accumulated precipitation are shown in Fig. 9. There are no large differences between the adiabatically and diabatically initialized forecasts.

Compared to both adiabatic and diabatic nonlinear normal-mode initialization schemes, one advantage of using digital filters (both ADFI and DDFI) is that the humidity field is consistently initialized along with the other prognostic fields. The fact that the humidity field is treated in the same way in the ADFI and DDFI schemes may, to some extent, explain the insensitivity of the model precipitation to the treatment of diabatic processes in the initialization scheme. A noise-free and better-organized humidity field contributes to the removal of the high-frequency noise from the forecast, although this contribution is not very significant in the present study.

The insensitive dependence discussed above may also be related to the particular scheme for condensation and clouds in the HIRLAM forecast model used in this study. The precipitation comes from cloud water content (CWC), which is a prognostic model variable in the same way as in Sundqvist et al. (1989). The analyzed CWC field has not been available in any operational context. Both DDFI and ADFI forecasts

TABLE 1. Root-mean-square (rms) and maximum differences in temperature, wind components, and surface pressure between the initialized and uninitialized analyses. For T, u, and v, the statistics are for the three-dimensional fields. DDFI − NOIN: changes due to diabatic digital filtering; ADFI − NOIN: changes due to adiabatic digital filtering.

	T (K)		u (m s^{-1})		v (m s^{-1})		p_s (hPa)	
	rms	max	rms	max	rms	max	rms	max
DDFI − NOIN	0.27	3.94	0.64	5.11	0.64	5.55	0.76	3.12
ADFI − NOIN	0.10	0.92	0.38	3.59	0.38	5.28	0.36	1.27

TABLE 2. Root-mean-square (rms) and maximum differences in temperature, wind components, and surface pressure between the 24-h forecasts starting from the initialized datasets and uninitialized forecast. For T, u, and v, the statistics are for the three-dimensional fields. DDFI − NOIN: changes due to diabatic digital filtering; ADFI − NOIN: changes due to adiabatic digital filtering.

	T (K)		u (m s^{-1})		v (m s^{-1})		p_s (hPa)	
	rms	max	rms	max	rms	max	rms	max
DDFI − NOIN	0.16	2.53	0.38	6.41	0.38	9.06	0.35	1.72
ADFI − NOIN	0.06	1.53	0.18	6.15	0.18	5.58	0.06	0.84

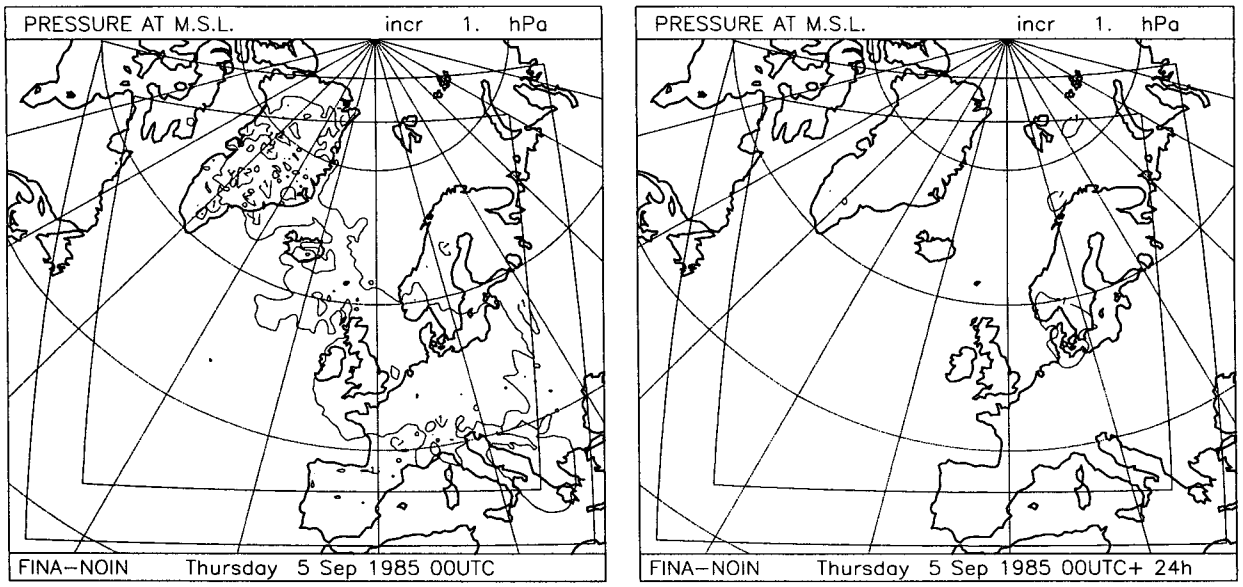

FIG. 7. (a) Difference in initial sea level pressure between DDFI analysis and the uninitialized analysis. (b) Difference in sea level pressure between the 24-h forecast from the DDFI analysis and that from the uninitialized analysis.

started from the same initial CWC field, namely, CWC = 0 everywhere. Therefore, the spinup of precipitation in the DDFI forecast is not very different from that of the ADFI forecast. One extension of the present DDFI scheme is to include a CWC field, which may influence the initial cloud distribution and precipitation. Preliminary work on defining the initial cloud water content has been reported by Kristjánsson (1991).

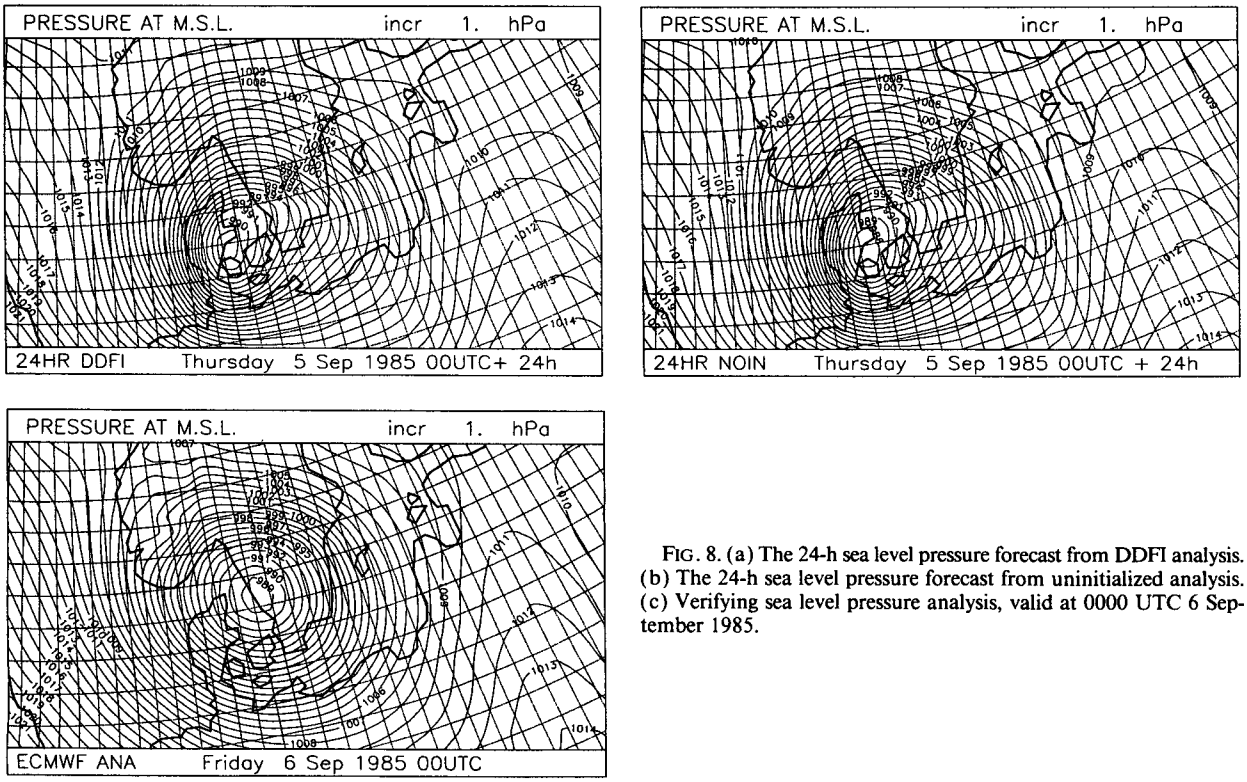

FIG. 8. (a) The 24-h sea level pressure forecast from DDFI analysis. (b) The 24-h sea level pressure forecast from uninitialized analysis. (c) Verifying sea level pressure analysis, valid at 0000 UTC 6 September 1985.

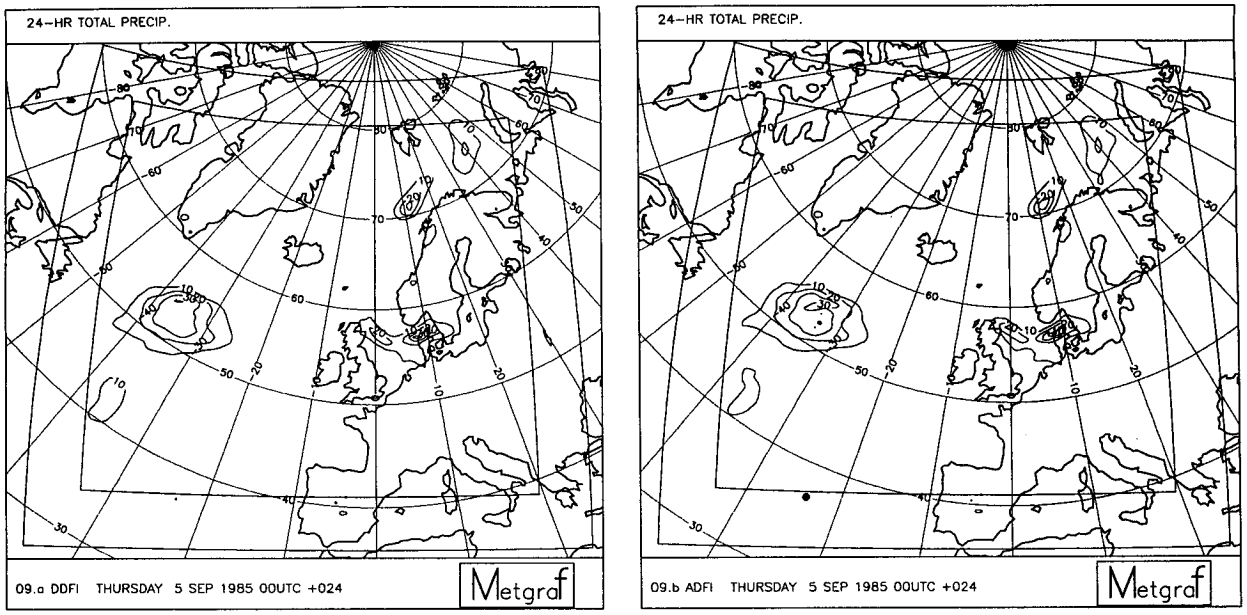

FIG. 9. Total accumulated precipitation (mm) for the 24-h period, produced by the forecast starting from (a) the DDFI analysis and (b) the ADFI analysis.

g. Hurricane Hugo

Hurricane Hugo is chosen here to demonstrate the applicability of ADFI and DDFI to different geographic locations and different synoptic weather situations. Hugo began as an easterly wave and reached hurricane strength by 1000 UTC 14 September 1989. During the period 0000 UTC 20–21 September, Hugo turned northwestward toward the continental United States. The timing of this turning was a critical forecast problem and a review of numerical forecasts for Hugo is given by Ward (1990). A study of Hugo with HIRLAM is being undertaken in a collaborative project between Colin Jones of the Climatic Research Unit, University of East Anglia, and the Department of Meteorology, University of Stockholm. The purpose of this study is to assess the impact of different physical processes (e.g., convection, condensation, and precipitation), initial-boundary condition resolution, and model resolution on the evolution of Hurricane Hugo. The full results will be reported in the near future. Here only the applications of ADFI and DDFI are briefly presented, and 6-h forecasts from ADFI and DDFI analyses are compared with that from uninitialized analysis.

The HIRLAM used in the Hugo experiments has a grid of $110 \times 100 \times 16$ points and a horizontal resolution $0.25° \times 0.25°$. The parameters are kept unchanged, except that the time step and the horizontal diffusivity are halved compared with the experiments presented outside this subsection.

The ECMWF analysis of the sea level pressure in the vicinity of Hurricane Hugo for 0000 UTC 18 September 1989 interpolated to the HIRLAM grid is shown in Fig. 10a. The area is dominated by a tropical storm with a minimum sea level pressure of 1003 hPa. Observations at this time put Hugo at a minimum sea level pressure of 946 hPa (Case and Mayfield 1990). Clearly the ECMWF analysis fails to produce a deep enough storm, possibly due to a combination of model defects, poor resolution, lack of observations for the analysis, and the analysis-rejecting data that was available.

The DDFI and ADFI analyses are shown in Figs. 10b and 10c, respectively. Both DDFI and ADFI produce smoother sea level pressure fields than the original uninitialized analysis. Some of the small-scale features due to the high-resolution orography may develop during the initializations. The central pressure of Hugo has been lowered 3 hPa by the DDFI. The shape of the low center has also been changed slightly by the initialization schemes. These changes are not discussed further in this paper and will be reported together with the Hugo project mentioned earlier.

In order to demonstrate the efficacy of ADFI and DDFI in suppressing the noise in the forecast, three short-range forecasts have been made. In Fig. 11, the mean absolute surface pressure tendency N_1 is shown for NOIN (forecast from uninitialized analysis), ADFI (forecast from ADFI analysis), and DDFI (forecast from DDFI analysis). It is clearly shown that the noise in the NOIN forecast has been effectively removed by both ADFI and DDFI. The two forecasts from initial-

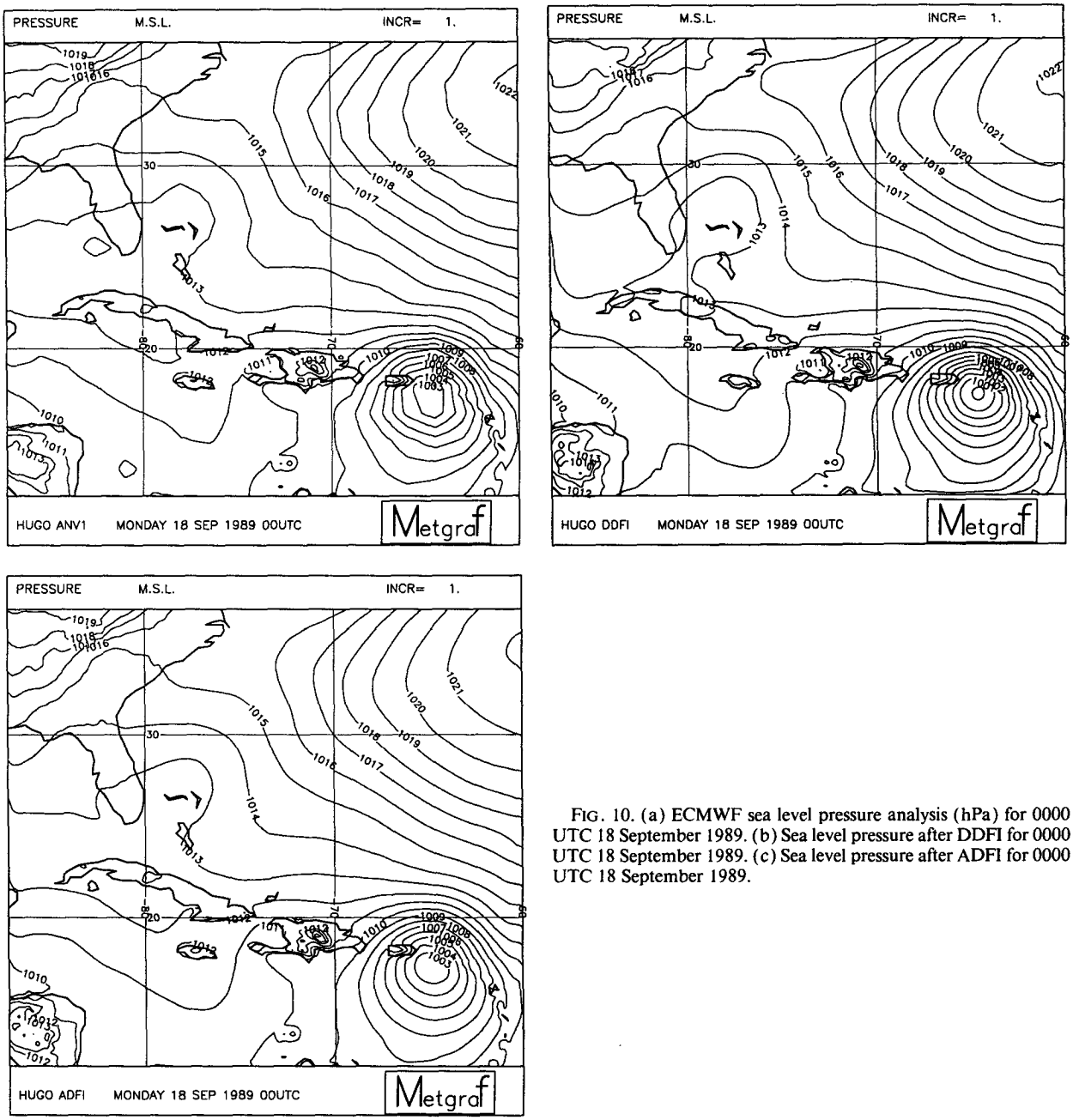

FIG. 10. (a) ECMWF sea level pressure analysis (hPa) for 0000 UTC 18 September 1989. (b) Sea level pressure after DDFI for 0000 UTC 18 September 1989. (c) Sea level pressure after ADFI for 0000 UTC 18 September 1989.

ized analyses show almost no noise in N_1, and DDFI appears to be slightly better than ADFI in this respect during the 6-h period.

4. Optimization of the filter

The computational expense of applying the digital-filtering technique depends directly on the length or order of the filter used. The objective of filter design is to achieve the required degree of filtering using a filter with the smallest number of coefficients. Two design methods are considered in the Appendix. The first is based on a Fourier decomposition of the ideal response, combined with a suitable *window* function; the second, based on the Chebyshev or minimax principle, yields a so-called optimal filter.

In section 4a, the minimum time span required to achieve a given frequency cutoff is considered. The response characteristics of the two types of filter are compared in section 4b; in general, optimal filters achieve

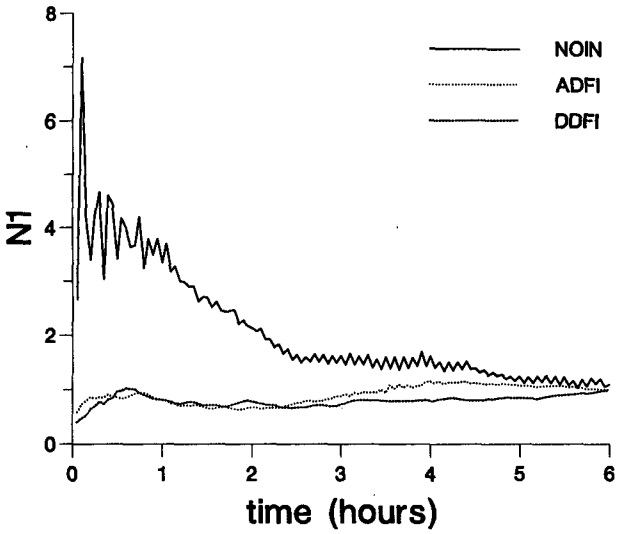

FIG. 11. Time evolution of the mean absolute surface pressure tendency averaged over the interior model domain [hPa (3 h)$^{-1}$] for the Hugo experiments.

the desired specifications for a lower order than those constructed using the simple window method. The implications for the computational efficiency of digital filtering are discussed in section 4c.

a. The minimum time span

The uncertainty principle plays a dominant role in the problem of meeting given specifications with a filter of limited length. This principle, first discovered by Heisenberg in connection with quantum mechanics, has much wider ramifications. In a general form, it places a limit on the extent to which a function $h(t)$ and its Fourier transform $H(\omega)$ can be simultaneously localized in their respective domains. The variances of the squared moduli in the time and frequency domains are defined by

$$\sigma_t^2 = \frac{\int_{-\infty}^{+\infty} t^2 hh^* \, dt}{\int_{-\infty}^{+\infty} hh^* \, dt}; \quad \sigma_\omega^2 = \frac{\int_{-\infty}^{+\infty} \omega^2 HH^* \, d\omega}{\int_{-\infty}^{+\infty} HH^* \, d\omega}.$$

The uncertainty relation (Bracewell 1978, p. 160) states that

$$\sigma_t \sigma_\omega \geq \frac{1}{2}.$$

For an ideal low-pass filter with cutoff frequency ω_c, the standard deviation $\sigma_\omega = \omega_c/\sqrt{3}$, so that

$$\sigma_t \geq \frac{\sqrt{3}}{2\omega_c} = \frac{\sqrt{3}\tau_c}{4\pi}.$$

Taking a nominal cutoff period $\tau_c = 6$ h gives $\sigma_t \geq 0.827$ h. The function $h(t)$ will typically extend to at least $2\sigma_t$ in both positive and negative directions; thus, the total time span T_s must be of the order of 3 h or greater. As something less than the ideal response is acceptable, some further reduction, perhaps to 2 h, may be possible.

For a discrete filter, the order and span are related by $(2N + 1)\Delta t = T_s$. The uncertainty principle places a lower limit on the order required to achieve a given cutoff. As the cutoff frequency is reduced, the amplitude of the side lobes increases in such a way that σ_ω remains above the minimum permitted value. This places a limit on the minimum order required to achieve a specified attenuation in the stop band. Optimal filter design ensures the best possible suppression in the stop band for a specified cutoff.

b. Comparison of filter responses

The frequency response of four filters is shown in Fig. 12. Two of the filters are constructed using a Lanczos window and two by means of the optimal-design technique (for details, see the Appendix). The solid graph is for a Lanczos filter with a nominal cutoff of 6 h and a span $T_s = 6$ h (the filter used in LH and in section 3). The dotted curve is for the optimal or equiripple filter with a span $T_s = 3$ h. It can be seen that the behavior in the transition region is quite similar for these two filters. However, the optimal filter has sidelobes with amplitude of about 0.1 (determined by the value of δ) in the stop band. The plots in Fig. 12a are linear and cover the range $0 \leq \theta \leq 1$ (where $\theta = \omega\Delta t$ is the digital frequency). The behavior in the pass band can more easily be seen in a plot with abscissa $\lambda = \log_2(\theta/\theta_c)$, as shown in Fig. 12b. This shows the transfer functions over a wider range of frequency and indicates that the response of the optimal filter in the pass band is acceptably close to the ideal. The remaining two curves in Fig. 12 are for the Lanczos filter with a nominal cutoff of 6 h and a span $T_s = 3$ h (dashed line) and the optimal filter with a span $T_s = 2$ h (dot–dash line). These two filters have similar response in the pass and transition bands. The optimal filter has equiripple oscillations in the stop band. What is clear from these curves is that if the stop-band ripples can be tolerated, the optimal filters have the required response in the pass band with shorter span than that required by the Lanczos filters.

c. Computational implications

The computation time required to apply the diabatic digital-filtering initialization amounted to 1590 s (on a CONVEX-220). The application involves a 3-h backward adiabatic integration followed by a 6-h forecast. The time taken by the normal-mode method with

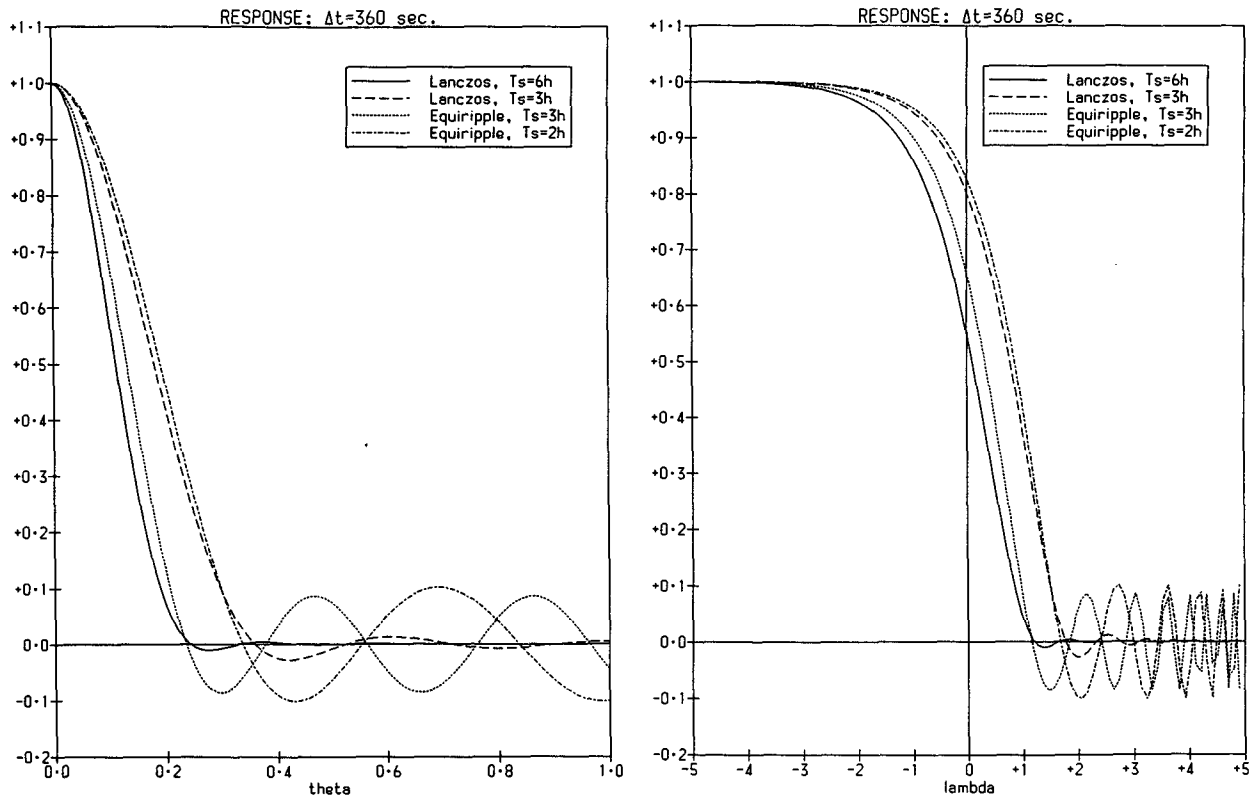

FIG. 12. Response functions for filters with coefficients defined as follows: (solid) $h_n = \sin(n\omega_c\Delta t)/n\pi$, with Lanczos window, cutoff $\tau_c = 2\pi/\omega_c$ of 6 h and span $T_s = 6$ h; (dashed) same, with span $T_s = 3$ h; (dotted) optimal filter with span $T_s = 3$ h; (dot–dash) optimal filter with span $T_s = 2$ h. (a) Abscissa linear, $0 < \theta < 1$; (b) abscissa $\lambda = \log_2(\theta/\theta_c)$.

two iterations for four vertical modes was 455 s. This does not include the computation of the eigenmodes; if these need to be calculated, the total time for the NMI scheme becomes 1149 s. The NMI scheme does not include diabatic effects; incorporation of these would increase the computation time significantly. For a fixed value of the time step, the time required for filtering is proportional to the filter span. Thus, a 50% reduction is achieved by using a filter with a 3-h span. If a 2-h span is adequate, a 67% saving results, bringing the computation time to 530 s: a value comparable to that required by the (adiabatic) normal-mode method. Such a short span is enabled by using an optimal filter. Further reduction is possible by increasing the time step since, for a given span, the time required for DFI varies inversely with Δt. Use of a semi-Lagrangian scheme for advection allows a larger time step to be used and enhances the appeal of the digital-filtering technique (Lynch 1990).

5. Further results and comments

The application of the initialization technique as described in section 3 employed a filter with a span T_s of 6 h. This involves a 3-h (backward) adiabatic integration followed by a 6-h diabatic forecast. While the results were satisfactory, the computational requirements of the method might, for some purposes, be considered excessive.

The computational cost is directly proportional to the filter span T_s. An obvious way to reduce the cost is to use a smaller value of T_s; however, the efficacy of the filter is diminished as the span is reduced. Therefore, it is important to choose the filter coefficients in such a way that adequate discrimination between low and high frequencies is obtained. The optimal filters described above ensure the best possible filter performance in a specific sense: for fixed-filter span and given pass-band and stop-band edges, the maximum deviation from the ideal in the pass band and stop band are minimized by this choice of filter.

The digital-filtering initialization technique was repeated, starting with the same uninitialized analysis, for a variety of different filters. The four filters depicted in Fig. 12 were used and the results compared. In Fig. 13, the evolution of the quantity N_1 for the forecasts from the corresponding four initializations are shown. The original filter, as used in section 3, is denoted LAN6 (Lanczos window, 6-h span). A similar filter, but with a 3-h span, is designated LAN3. It is clear

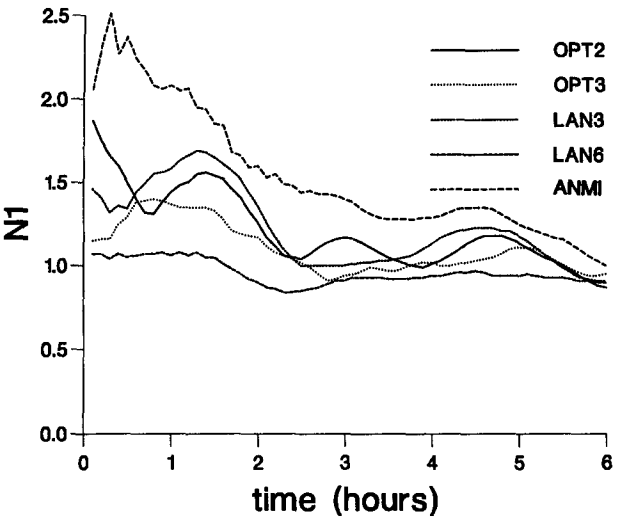

FIG. 13. Time evolution of the mean absolute surface pressure tendency N_1 for analyses initialized by four different digital filters and for nonlinear normal-mode initialization (ANMI).

that this filter is less effective in removing the high-frequency noise from the forecast: the initial value of N_1 is higher and rises to a value of about 1.7 before falling again. The curve denoted OPT3 is for the optimal filter with a 3-h span: the forecast noise for this filter, as measured by N_1, is intermediate between the values for the two Lanczos filters. The curve marked OPT2 is for the optimal filter with a 2-h span: here the values of N_1 are larger than for OPT3, and there is clear evidence of residual high-frequency noise. The performance of this filter is comparable to LAN3.

The fifth graph in Fig. 13 is for the forecast starting from an analysis initialized using an adiabatic nonlinear normal-mode method (ANMI). It can be seen that all four of the digital filters are superior to the ANMI in reducing the high-frequency noise. The initial tendency of surface pressure for the OPT3 filter is shown in Fig. 14a. The field is somewhat noisier than for the LAN6 filter (Fig. 5a) but, by and large, synoptically reasonable. With the span of the optimal filter reduced to 2 h (OPT2), the initial tendency becomes that in Fig. 14b; the values are now noticeably larger and the field more noisy. However, the values are still much smaller and more reasonable than those resulting from the ANMI method, which are shown in Fig. 5c.

In conclusion, it seems that the cost of applying the digital-filtering procedure can be significantly reduced by using a filter of optimal design. The OPT3 filter requires only one-half the computational cost compared with the filter used in section 3. If the small residual noise is acceptable, the OPT2 filter needs only one-third of the original computation time. Even this filter yields results superior to the nonlinear normal-mode method (ANMI).

In addition to spurious gravity wave activity in the analysis, high frequencies are generated continuously during the model integration. Generally, these oscillations are small, but they may cause problems when the diabatic forcing is locally intense. Such noise could

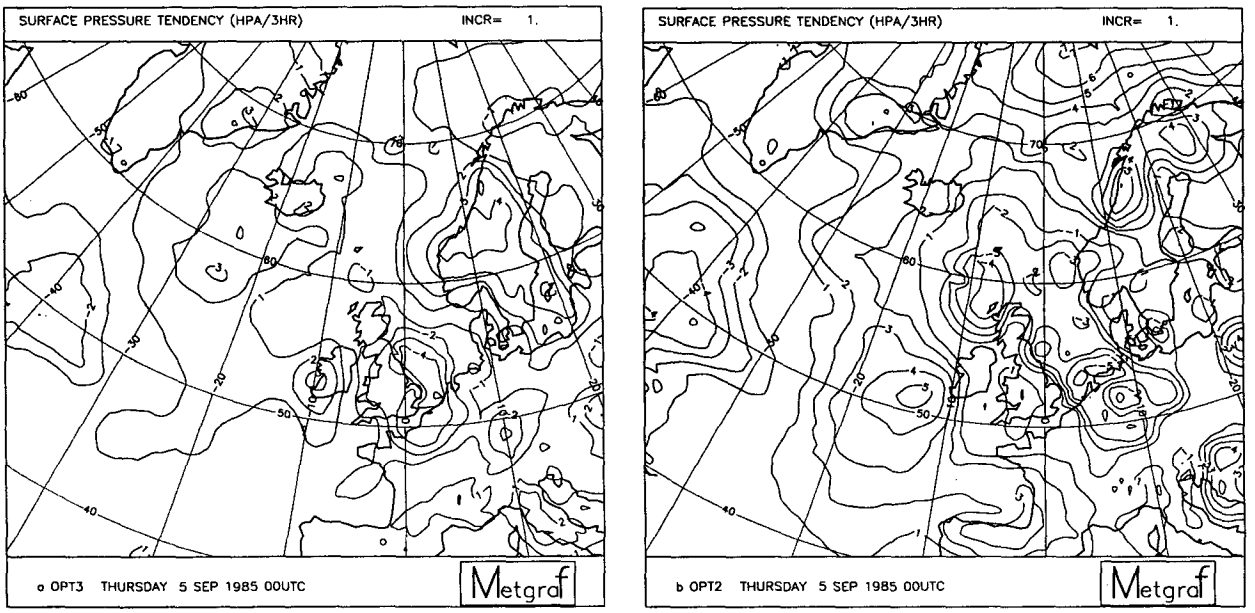

FIG. 14. Initial surface pressure tendency [hPa (3 h)$^{-1}$] for the analysis initialized by DDFI using (a) the OPT3 filter and (b) the OPT2 filter.

be controlled by repeated application of a filter. The nonrecursive filters considered in this study would probably prove computationally prohibitive. A recursive filter, which allows for feedback of previous outputs, would seem more suitable and would achieve the desired filtering more economically. The combination of a recursive filter with a time integration scheme can markedly change the stability characteristics of the scheme. Further investigation of this problem, which is of particular interest in climate modeling, is necessary.

6. Conclusions

The digital-filtering initialization scheme used by Lynch and Huang (1991), referred to as LH throughout this study, is extended to include diabatic processes. As in LH, the digital filter is applied to a time series to remove the spurious high-frequency oscillations due to the imbalance between the initial fields of mass and wind. In the present study, however, the time series is obtained from diabatic integration of the numerical model. In order for the time series to be centered around the initial time, integration backward in time is needed; since the diabatic processes are irreversible, the backward integration has to be adiabatic. Therefore, the procedure is to first integrate the model adiabatically backward for one-half of the filter span and to follow this by a diabatic integration for the full span in order to generate the time series to which the digital filter is applied.

The diabatic digital-filtering initialization (DDFI) and the adiabatic digital-filtering initialization (ADFI) remove the spurious high-frequency oscillations from the forecast very efficiently. The former gives a lower noise level and a significantly smoother structure in surface pressure tendency than the latter does. The improvements occur mainly in mountainous regions. The modifications made by DDFI to the initial fields are somewhat larger than for ADFI but are of the same order of magnitude. These changes are generally much smaller than the observational error. The changes made by DDFI to the 24-h forecast are also larger than for ADFI. However, the rms changes in the forecast are smaller than those induced in the analysis by the diabatic initialization.

There are some problems related to the boundary relaxation scheme that need further investigation, but the conclusions from this study will not be changed as long as the weather systems of interest are within the interior of the model domain. The initialization of the cloud-water content discussed in this paper is certainly an interesting problem that will be investigated next.

DDFI needs more CPU time than ADFI, due to the 6-h diabatic integration; however, it is possible to use a shorter filter span for operational purposes. A shorter span will tend to give rise to a higher noise level during the first few hours of the forecast; however, this problem can be ameliorated by use of an optimal filter design. By this means it is possible to construct a digital filter that gives acceptable results with a span as short as 2–3 h.

Since diabatic processes are relatively more important in the tropics, it would be of interest to compare DDFI and ADFI with a global model or by running HIRLAM over the tropics. Preliminary results of the Hurricane Hugo case have been presented; further studies of tropical circulations with HIRLAM are being undertaken and will be reported later.

Acknowledgments. We are grateful to Dr. Erland Källén and Prof. Hilding Sundqvist for carefully reading the manuscript and for constructive discussions. We also want to thank Colin Jones for his help in the numerical experiments on the Hugo case. This study was partially supported by NFR (Swedish National Science Research Council) Contracts G-GU 1705-311 and E-EG 2923-302.

APPENDIX

Two Filter-Design Methods

a. Design by windowing

The filter coefficients used in Lynch and Huang (1992; LH) and in sections 2 and 3 were obtained using the simplest design technique for a nonrecursive filter: the *window method.* The desired frequency response is chosen, typically that of an ideal low-pass filter:

$$H(\theta) = \begin{cases} 1, & |\theta| \leq |\theta_c|; \\ 0, & |\theta| > |\theta_c|, \end{cases} \tag{A1}$$

where θ_c is a cutoff frequency. This is expanded as a Fourier series

$$H(\theta) = \sum_{n=-\infty}^{\infty} h_n e^{-in\theta}; \quad h_n = \frac{1}{2\pi}\int_{-\pi}^{\pi} H(\theta) e^{in\theta} d\theta. \tag{A2}$$

The values of the coefficients h_n follow immediately from (A1) and (A2):

$$h_n = \frac{\sin n\theta_c}{n\pi}. \tag{A3}$$

These coefficients are the weights used to filter an input function $f_n = f(n\Delta t)$ by convolution

$$f_n^* = (h*f)_n = \sum_{k=-\infty}^{\infty} h_k f_{n-k}. \tag{A4}$$

The output f^* is the low-frequency component of f_n. The sequence $\{h_n\}$ is known as the impulse response;

it is the output of the filter for an input consisting of a unit pulse at time zero.

In practice, only a finite number of coefficients can be used. Thus, the nonrecursive filter acquires its alternative name finite impulse response or FIR filter. Truncation of the Fourier series (A2) is equivalent to multiplication of the sequence $\{h_n\}$ by a *window function* $\{w_n\}$ defined by

$$w_n = \begin{cases} 1, & |n| \leq N; \\ 0, & |n| > N. \end{cases} \quad \text{(A5)}$$

In view of its graph, this particular function $\{w_n\}$ is called the rectangular or uniform window. The stop band and pass band of the filter are then separated by a transition band whose width depends upon the truncation limit N. It is well known that the sudden discontinuity in the rectangular window gives rise to spurious oscillations in the resulting response function. These *Gibbs oscillations* are greatly reduced if a window with a more gentle cutoff at $n = N$ is used. In LH, a Lanczos window

$$w_n = \frac{\sin[n\pi/(N+1)]}{n\pi/(N+1)}$$

was used. A large number of other windows have been proposed and several of them are discussed in Oppenheim and Schafer (1989). The Kaiser window has the advantage of an adjustable parameter that can be chosen to achieve specified filter characteristics. However, all the windows reduce Gibbs oscillations at the cost of widening the transition band of the filter.

b. *Optimal FIR filters*

Optimal FIR filters have the smallest maximum approximation error for a prescribed transition band. The theory of these filters, which rests on the Chebyshev alternation theorem, is presented by Oppenheim and Schafer (1989), and an algorithm for deriving the filter coefficients is described there. An outline of the theory will be given below.

Let $H(\theta)$ be the desired or ideal filter-frequency response and $H_N(\theta)$ that of a filter of total span $(2N + 1)\Delta t$. The design method using Fourier series truncated by a rectangular window (A5) corresponds to minimizing the L_2 norm of the error:

$$\|E\|_2^2 = \frac{1}{2\pi}\int_{-\pi}^{\pi} |H(\theta) - H_N(\theta)|^2 d\theta. \quad \text{(A6)}$$

However, this criterion may result in adverse behavior near discontinuities of $H(\theta)$: a minimum mean squared error does not preclude large localized errors. Optimal filter design employs an alternative minimization criterion using the L_∞ norm

$$\|E\|_\infty = \max|H(\theta) - H_N(\theta)|. \quad \text{(A7)}$$

The Chebyshev or minimax criterion seeks a response $H_N(\theta)$ such that this *maximum* error (within the pass band and stop band, not the transition band) is *minimized.* Thus, the "worst error" is as small as possible and large local errors are prevented. The response function, which minimizes the maximum error (A7), may be found by an iterative procedure called the Remez exchange algorithm. The mathematical theory of the method is presented in Esch (1990).

For filters designed by the windowing method, the errors tend to be maximum close to points of discontinuity of the ideal response. The optimal filters minimize the maximum deviation from the ideal and the error is spread more evenly throughout the range of frequencies. This property accounts for their description as *equiripple* filters. Several interesting properties of these filters are described by Oppenheim and Schafer (1989). A software package DF-PAK, which includes code for the calculation of the optimal filter coefficients, is contained in Taylor and Stouraitis (1987). [A Fortran source code can be found in McClellan et al. (1973) and is also available from the corresponding author.]

The DF-PAK software was used to design optimal filters for initialization. Two such designs are presented in section 4b, with spans of 3 and 2 h, respectively. The pass-band edge ω_p was set to correspond to a period of 12 h. Then the truncation N, such that $(2N + 1)\Delta t = T_s$, was fixed and the stop-band edge ω_s varied until the deviation from the ideal response satisfied the conditions

$$|H(\omega) - 1| \leq \delta, \quad 0 \leq \omega \leq \omega_p;$$
$$|H(\omega)| \leq \delta, \quad \omega_s \leq \omega \leq \pi/\Delta t.$$

The error δ was set at 0.1. In engineering terms, the gain is defined in decibels (dB) as

$$G = -10 \log_{10}|H(\omega)|^2,$$

so that, with the chosen value of δ, the attenuation in the stop band is at least 20 dB. This implies that the energy of components in the stop band $(\omega_s, \pi/\Delta t)$ is reduced to less than 1% of its initial value.

REFERENCES

Baer, F., 1977: Adjustment of initial conditions required to suppress gravity oscillations in nonlinear flows. *Beitr. Phys. Atmos.*, **50,** 350–366.

Bracewell, R. N., 1978: *The Fourier Transform and Its Applications.* McGraw-Hill, 444 pp.

Case, B., and M. Mayfield, 1990: Atlantic hurricane season of 1989. *Mon. Wea. Rev.*, **118,** 1165–1177.

Esch, R., 1990: Functional Approximation. *Handbook of Applied Mathematics,* C. E. Pearson, Ed., Van Nostrand Reinhold, 928–987.

Fox-Rabinovitz, M. S., and B. D. Gross, 1991: Diabatic dynamic initialization for the GLA 4-D data assimilation system. Preprints, *Ninth Conf. on Numerical Weather Prediction,* Denver, Amer. Meteor. Soc., 373–376.

Kållberg, P., Ed., 1989: The HIRLAM level 1 system. Documentation Manual, 160 pp. [Available from SMHI, S-601 76 Norrköping, Sweden.]

Kitade, T., 1983: Nonlinear normal-mode initialization with physics. *Mon. Wea. Rev.*, **111,** 2194–2213.

Kristjánsson, J. E., 1991: Initialization of cloud water in a weather prediction model. Preprints, *Ninth Conf. on Numerical Weather Prediction,* Denver, Amer. Meteor. Soc., 823–824.

Lynch, P., 1985: Initialization of a barotropic limited-area model using the Laplace transform technique. *Mon. Wea. Rev.*, **113,** 1338–1344.

——, 1990: Initialization using a digital filter. *Research Activities in Atmospheric and Ocean Modeling,* CAS/JSC Working Group on Numerical Experimentation. Report No. 14, WMO Secretariat, Geneva, 1.5–1.6.

——, and X.-Y. Huang, 1992: Initialization of the HIRLAM model using a digital filter. *Mon. Wea. Rev.*, **120,** 1019–1034.

McClellan, J. H., T. W. Parks, and L. R. Rabiner, 1973: A computer program for designing optimum FIR linear phase digital filters. *IEEE Trans. on Audio and Electroacoustics.* Vol. AU-21, No. 6, 506–526.

Machenhauer, B., 1977: On the dynamics of gravity oscillations in a shallow water model with applications to normal mode initialization. *Beitr. Atmos. Phys.*, **50,** 253–271.

Miyakoda, K., and R. W. Moyer, 1968: A method of initialization for dynamical weather forecasting. *Tellus,* **20,** 115–128.

Oppenheim, A. V., and R. W. Schafer, 1989: *Discrete-Time Signal Processing.* Prentice-Hall International, 879 pp.

Phillips, N. A., 1960: On the problem of initial data for the primitive equations. *Tellus,* **12,** 121–126.

Semazzi, F. H. M., and I. M. Navon, 1986: A comparison of the bounded derivative and the normal-mode initialization methods using real data. *Mon. Wea. Rev.*, **114,** 2106–2121.

Sundqvist, H., E. Berge, and J. E. Kristjánsson, 1989: Condensation and cloud parameterization studies with a mesoscale numerical weather prediction model. *Mon. Wea. Rev.*, **117,** 1641–1657.

Taylor, F. J., and T. Stouraitis, 1987: *Digital Filter Design Software for the IBM PC.* Marcel Dekker, 299 pp.

Temperton, C., and D. L. Williamson, 1981: Normal-mode initialization for a multilevel gridpoint model. Part 1: Linear aspects. *Mon. Wea. Rev.*, **109,** 729–743.

Ward, J. H., 1990: A review of numerical forecast guidance for Hurricane Hugo. *Wea. Forecasting,* **5,** 416–432.

Wergen, W., 1988: The diabatic ECMWF normal mode initialization scheme. *Beitr. Atmos. Phys.*, **61,** 274–302.

Williamson, D. L., and C. Temperton, 1981: Normal-mode initialization for a multilevel gridpoint model. Part 2: Nonlinear aspects. *Mon. Wea. Rev.*, **109,** 744–757.